Journal of Solid State Chemistry 182 (2009) 2149–2156

Contents lists available at ScienceDirect

Journal of Solid State Chemistry

journal homepage: www.elsevier.com/locate/jssc

Mechanosynthesis of nanopowders of the proton-conducting electrolyte material Ba(Zr, Y)$O_{3-\delta}$

I. Antunes [a,b], A. Brandão [a], F.M. Figueiredo [b], J.R. Frade [b], J. Grácio [a], D.P. Fagg [a,*]

[a] Nanotechnology Research Division, Centre of Mechanical Technology and Automation, University of Aveiro, 3810-193 Aveiro, Portugal
[b] Department of Ceramics and Glass Engineering, CICECO, University of Aveiro, 3810-193 Aveiro, Portugal

ARTICLE INFO

Article history:
Received 11 February 2009
Received in revised form
20 May 2009
Accepted 24 May 2009
Available online 31 May 2009

Keywords:
Barium zirconate
$BaZrO_3$
Mechanosynthesis
Nanopowders
Perovskite
Proton conductor

ABSTRACT

The formation of perovskite nanopowders of the common proton-conducting, electrolyte material $Ba(Zr_{1-x}Y_x)O_{3-\delta}$ is demonstrated by room temperature mechanosynthesis for the compositional range $x = 0$, 0.058 and 0.148. This is achieved with a planetary ball mill at 650 rpm in zirconia vials, starting from BaO_2 with ZrO_2, $(ZrO_2)_{0.97}(Y_2O_3)_{0.03}$ or $(ZrO_2)_{0.92}(Y_2O_3)_{0.08}$ precursors, respectively. Powder X-ray diffraction (XRD) reveals the formation of the perovskite phase in the early stages of milling with phase purity being achieved after milling times of 240 min for composition $x = 0.058$ whereas 420 min is necessary for composition $x = 0.148$. In contrast, traces of ZrO_2 are apparent in composition $x = 0$ even after milling times of 420 min. The use of $BaCO_3$ as precursor does not allow the formation of the perovskite phase for any composition. The perovskite crystallites are spherical in shape with an average size determined from XRD of ca. 30 nm in agreement with transmission electron microscopy observations. FTIR spectra demonstrate that contamination levels of $BaCO_3$ in the mechanosynthesized powders are very low. The spherical shape and nanoscale of the crystallites allow densification levels that are highly competitive when compared to $BaZrO_3$-based materials formed by alternative synthesis techniques documented in the literature.

© 2009 Elsevier Inc. All rights reserved.

1. Introduction

In recent years, perovskite, proton conducting, electrolyte materials based on the cerates or zirconates of barium doped with yttrium or lanthanide oxides have been extensively studied for application in intermediate temperature fuel cells, electrolysis cells, sensors and hydrogen pumps. The zirconate materials in particular have created immense interest due to high levels of proton conductivity coupled with superior stability in steam or CO_2 containing atmospheres. Trivalent doped barium zirconate can be synthesized by a classical solid state synthesis method starting from $BaCO_3$, ZrO_2 and Y_2O_3; however, powders prepared by this approach are repeatedly shown to offer lack of reproducibility, producing relatively large and varied grain sizes, strong agglomeration and no guarantee of compositional homogeneity [1,2]. Authors using this technique have typically been forced to resort to subsequent repeated grinding steps to achieve pure phases and particle size reduction. Furthermore, due to their refractory nature, barium zirconate based materials are notoriously difficult to sinter, typically requiring sintering temperatures as high as 1700–1800 °C to achieve full densities. These extreme conditions prevent easy implementation of these materials in fuel cells and other devices, preventing fabrication of co-sintered structures, adding to overall costs, causing abnormal grain growth [2,3] and also causing barium oxide evaporation [1,4,5]. To overcome these difficulties soft chemical routes have become increasing important for the formation of barium zirconate materials. In general these methods offer the benefits of low synthesis temperatures and the possibility of producing ultrafine powders. A wide range of soft chemistry techniques have been employed to form barium zirconate based materials such as, co-precipitation [6–8], hydrothermal synthesis [9,10], sol–gel techniques [11–14], thermal decomposition of nitrate [15], spray pyrolysis [16,17] and combustion synthesis [4,12]. However, several disadvantages have been noted with many of these techniques such as, the evaporation of solvents due to non-homogeneity causing the formation of segregation phases or alteration of stoichiometry due to incomplete precipitation processes [18], expensive chemicals and time consuming processes [11–14] and the discharge of pollutant gases [4,6,12,15]. Furthermore, the formation of $BaCO_3$ as an impurity phase on decomposition of organics is a common occurrence in many of these processes which requires additional calcinations steps to remove and may add to compositional inhomogeneity [4,6,12,14,15,18].

The current work reports the formation of $BaZr_{1-x}Y_xO_{3-\delta}$ nanopowders by room temperature mechanosynthesis for the first time. The mechanosynthesis technique offers a cheap, quick

* Corresponding author. Fax: +351 234 425 300.
E-mail address: duncan@ua.pt (D.P. Fagg).

0022-4596/$ - see front matter © 2009 Elsevier Inc. All rights reserved.
doi:10.1016/j.jssc.2009.05.027

and efficient method with which to achieve highly reactive, homogeneous, nanopowders. Previous authors have demonstrated room temperature mechanosynthesis of the comparable perovskite material $BaTiO_3$ by use of a standard planetary mill at 200 rpm for BaO_2 and TiO_2 precursors [19]. Other authors have shown that $BaCO_3$ and TiO_2 precursors can be reacted by use of a very high energy steel mill operating at 4000 rpm [20]. For the barium zirconate system a two step process of mechanical activation with an additional annealing step has been suggested to produce the perovskite phase [21]. In contrast, the current article documents successful one step mechanosynthesis of $BaZr_{1-x}Y_xO_{3-\delta}$ materials for compositions $x = 0$, 0.058 and 0.148. Work is presented together with an appraisal of how this technique may resolve many of the limitations presently suffered by alternative synthesis techniques, while outlining the precautions necessary to minimize contamination.

2. Experimental

Powders of $BaZr_{1-x}Y_xO_{3-\delta}$ ($x = 0$, 0.058 and 0.148) were prepared by mechanosynthesis from stoichiometric quantities of precursors mixtures: barium peroxide (Riedel-de-Häen, 95% purity), with, respectively, high purity zirconium (IV) oxide (Riedel-de-Häen, 99% purity), $(ZrO_2)_{0.97}(Y_2O_3)_{0.03}$ (TOSOH Co.) and $(ZrO_2)_{0.92}(Y_2O_3)_{0.08}$ (TOSOH Co.). Initial particle sizes of the zirconium-containing powders were about 200 nm for the pure ZrO_2 and in the range 60–80 nm for the Y-substituted compositions, as determined by surface area measurements. For this reason the monoclinic ZrO_2 precursor was milled for 60 min to bring down the particle size to the comparable size of 80 nm. X-ray diffraction (XRD) analysis confirmed that no phase changes were induced by this operation under the current milling conditions. The commercial powder of barium peroxide was found to be a mixture of 95 mol% BaO_2 with 5 mol% $BaCO_3$, the exact quantities of which were confirmed by thermogravimetric analysis in flowing CO_2 using a SETARAM TG-DTA/DSC Labsys Instrument with a 1600 °C rod. The initial particle sizes of BaO_2 and $BaCO_3$ precursors are 10–20 and 0.5 μm, respectively. The milling experiments were conducted in a planetary ball mill (Retsch PM200) with constant planetary rotation of 650 rpm using 125 cm^3 tetragonal zirconia vials (Retsch) and balls (Tosoh Co.). The ball to powders weight ratio was ~10:1. Excess heating was avoided by milling for periods of 5 min with a subsequent pause for the same period of time. After each interruption, the direction of rotation was reversed. No special atmospheres were used during grinding. Progression of reaction was monitored by XRD analysis of powder samples collected at regular periods of time, using a Rigaku Geigerflex diffractometer (Cu$K\alpha$ radiation, step width 0.02°, scan rate 1°/min). The strain and diffracting volume contributions to peak broadening were assessed by an integral breadth method based on Williamson–Hall plots [22]. The experimental width was corrected based on data collected for LaB_6 standard reference. Ceramic samples were obtained by isostatically pressing the synthesized powders at 200 MPa with subsequent sintering in air at temperatures of 1300, 1400, 1500 and 1600 °C, for 5 and 10 h with heating rate 5 °C/min. Density was measured by the Archimedes method by immersion in diethyl phthalate, and by geometric measurements; the latter being 3–4% lower than the Archimedes values, for the densest samples. The microstructure and chemical homogeneity of the powders were analysed by transmission electron microscopy (TEM) coupled with energy dispersive X-ray spectroscopy (EDS) in a 300 kV Hitachi H-9000 microscope with Röntec EDS detector. Samples were prepared by dispersing in ethanol and supporting on perforated copper grids. Average grain sizes were estimated from equivalent circular diameters measured on TEM and SEM digital micrographs upon suitable processing and analysed with ImageJ 1.37v software (Wayne Rasband, National Institutes of Health, USA). Zirconia contamination was monitored by inductively coupled plasma-atomic emission spectroscopy (ICP-AES) analysis (Jobin Yvon 70 Plus spectrometer) of solutions of the milled powders which had been dissolved in acid mixtures in an ultrasonic bath. Room temperature infrared absorption spectra were recorded using a Spectrum-1000 Fourier transform infrared (FT-IR) instrument (Perkin-Elmer). The spectra were collected in the range of 300–2000 cm^{-1} using a KBr pellet.

3. Results and discussion

3.1. Phase formation

The evolution of the perovskite phase is shown by the XRD data in Fig. 1A, B and C, for compositions $BaZr_{1-x}Y_xO_{3-\delta}$ ($x = 0$, 0.058 and 0.148, respectively) as a function of milling time. For each composition, the onset of perovskite phase formation can be observed after 60 min. Further milling leads to substantial increases in intensity of the perovskite reflections indicating that mechanochemical reaction takes place at room temperature. Reaction appears to occur more rapidly in the case of $x = 0.058$ with the pure perovskite phase attained after approximately 240 min. In contrast, phase purity in composition 0.148 requires the longer milling time of 420 min (Fig. 2A), while composition $x = 0$ exhibits small traces of monoclinic zirconia as an impurity phase in the XRD patterns throughout all milling times investigated (Figs. 1A and 2A).

ICP-AES studies have been performed to confirm nominal stoichiometry, Table 1. No trend can be observed which relates Zr-content to milling time and the materials studied are shown to have compositions equal to their nominal stoichiometries within the detection limit of the ICP-AES technique. Zirconia milling contaminations, if present, are, therefore, less than 1 mol%, which is in agreement with a maximum of 0.5 wt% Zr contamination found in powders of $Ca(Ti, Mn)O_{3-\delta}$ mechanosynthesized in similar conditions [23]. The persistent presence of zirconia in composition $x = 0$ may instead be due to incomplete reaction of $BaCO_3$, present as a trace impurity phase in the commercial barium peroxide precursor. Confirmation of this hypothesis is made by annealing the mechanosynthesized, $x = 0$, powder at 1250 °C for 5 h. The XRD pattern shown in Fig. 2B shows a clean pattern of $BaZrO_3$ with no impurity phases and symmetrical peaks suggesting homogeneity. Indeed, Fig. 3 demonstrates that mechanochemical reaction does not occur when using $BaCO_3$ as a precursor; the starting materials monoclinic zirconia and $BaCO_3$ are retained even for milling times in excess of 690 min, with no appearance of the perovskite phase. This probably reflects the higher thermodynamic stability of $BaCO_3$ with respect to BaO_2, as determined by using a suitable database and corresponding software (FactSage, GTT Technologies). The free energy change for the formation of $BaZrO_3$ from monoclinic ZrO_2 and these precursors at standard temperatures and pressures is $\Delta G_R^\circ = 24.2$ kcal/mol for $BaCO_3$ and -14.3 kcal/mol for BaO_2, showing that reaction is thermodynamically favourable for BaO_2 and unfavourable for $BaCO_3$ under these conditions. Haile et al. pointed out that undoped $BaZrO_3$ has a very low tolerance to *A*-site deficiency in contrast to the aliovalent doped compositions [5]. Hence, minor deviations from stoichiometry due to the trace presence of unreacted $BaCO_3$ in the commercial BaO_2 powder would be likely to cause the appearance of zirconia as an impurity phase in the composition $x = 0$, while a comparable

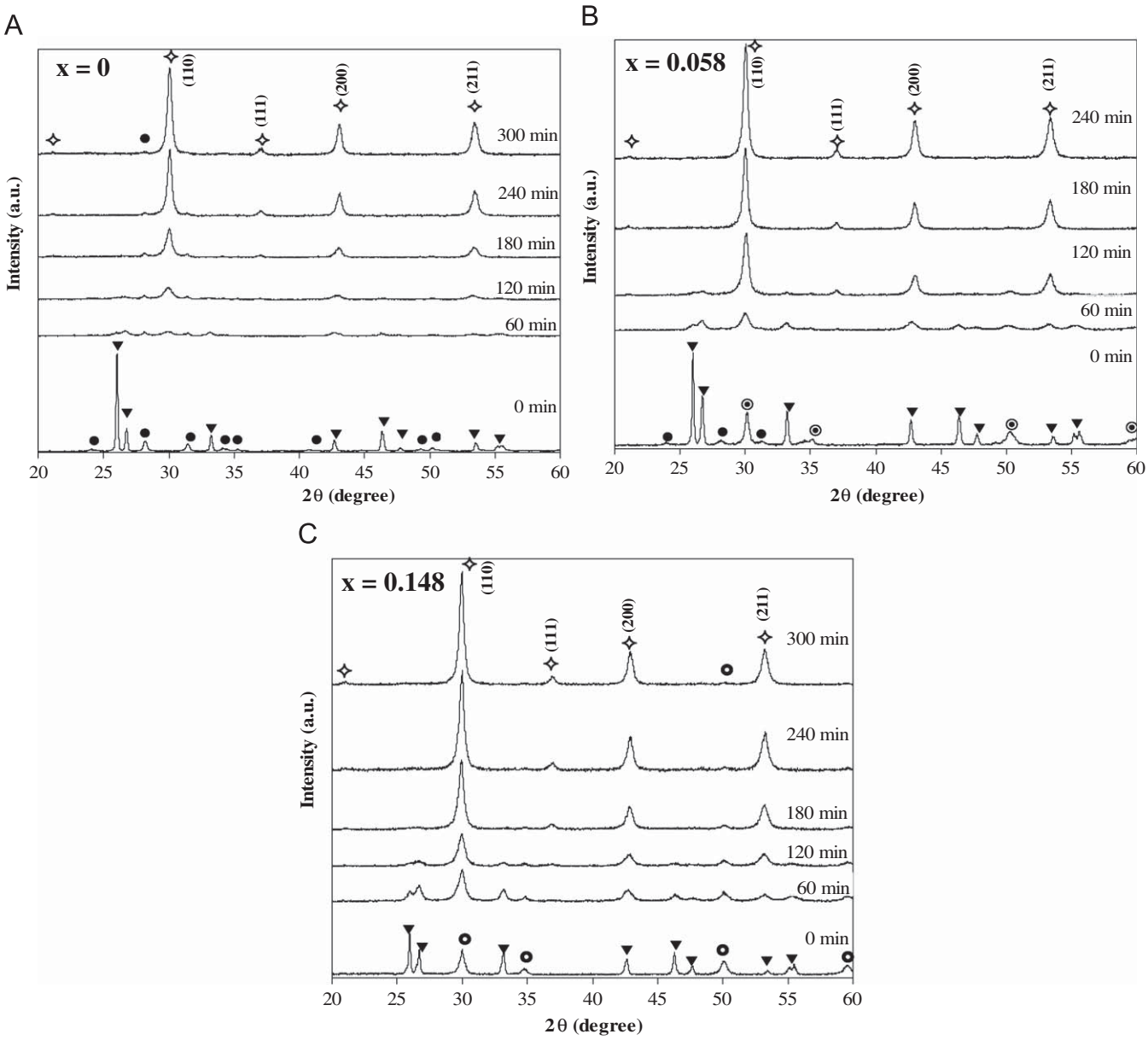

Fig. 1. Evolution of powder X-ray diffraction patterns with milling time for $BaZr_{1-x}Y_xO_{3-\delta}$ compositions (A) $x = 0$, (B) $x = 0.058$, (C) $x = 0.148$ for BaO_2+ZrO_2, $(ZrO_2)_{0.97}(Y_2O_3)_{0.03}$ or $(ZrO_2)_{0.92}(Y_2O_3)_{0.08}$ precursors, respectively. The markers identify (▼) barium peroxide; (◉, ◯) yttria doped zirconia (3 and 8 mol%, respectively); (●) monoclinic zirconia; (✧) perovskite phase.

compositional variation may be masked in the aliovalent doped compositions due to higher tolerances of Ba-deficiency.

The time necessary for perovskite phase formation was observed to be shortest for the composition $x = 0.058$. This interesting phenomenon is under further investigation by the authors with special reference to the crystallographic symmetry of the Zr-containing precursor. Table 2 summarizes lattice parameters of all mechanosynthesized compositions.

The milling energy needs to be high for the mechanochemical reaction to progress. For example, the use of nylon vials rather than zirconia vials is unsuccessful for mechanosynthesis, with no perovskite phase formation for milling times in excess of 420 min for even the most reactive starting materials. This is probably due to absorption of milling energy by vial deformation (results omitted for clarity).

Another interesting factor is the influence of the formed oxygen on the mechanochemical reaction. The progression of the reaction between BaO_2 and ZrO_2 yields oxygen as described:

$$BaO_2 + ZrO_2 \Leftrightarrow BaZrO_3 + \tfrac{1}{2}O_2\uparrow \quad (1)$$

Previously, the zirconia vial was opened after each 60 min of milling to obtain the results shown in Figs. 1 and 2. This repeated opening of the vial releases the oxygen allowing the reaction described by Eq. (1) to progress to the right. In contrast, when the formed O_2 is prevented from escaping (by keeping the vial sealed) the mechanochemical reaction is seriously retarded, Fig. 4.

3.2. Microstructure

All XRD patterns exhibit peak broadening which may arise due to the combined effect of a crystallite size in the nanometric range and lattice strain, both typical consequences of high energy milling. The lattice strain induced by milling may be taken into

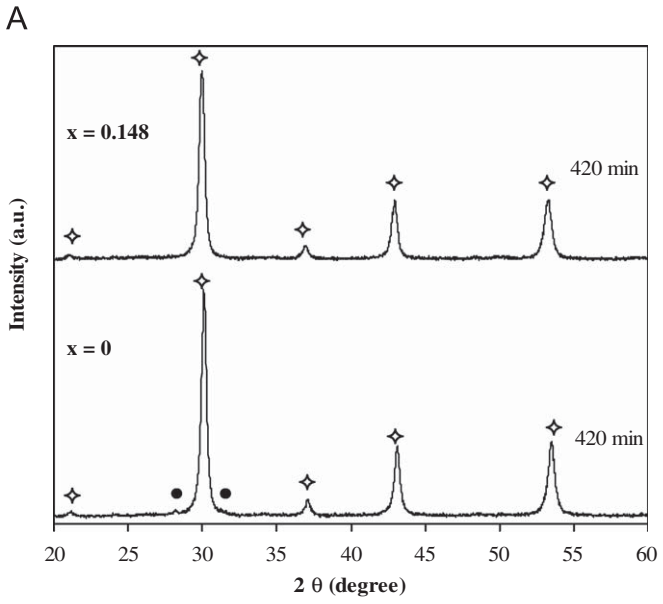

Fig. 2. (A) XRD pattern for $BaZr_{1-x}Y_xO_{3-\delta}$ ($x = 0$ and 0.148) after 420 min milling time, highlighting perovskite phase purity in $x = 0.148$, and a monoclinic ZrO_2 impurity in $x = 0$. (B) XRD pattern of $x = 0$ powder calcined at 1250 °C proving that the presence of monoclinic zirconia in $x = 0$ is due to incomplete mechanochemical reaction. The markers identify (▼) barium peroxide; (●) monoclinic zirconia; (✧) perovskite phase.

Table 1
Summary of chemical analysis by plasma-atomic emission spectroscopy (ICP-AES) of $BaZr_{1-x}Y_xO_{3-\delta}$ powders prepared by mechanosynthesis.

Composition x	Milling time (min)	Ba (mol/f.u.)	Y (mol/f.u.)	Zr (mol/f.u.)
0	420	0.99	–	1.00
0.058	300	0.99	0.06	0.94
0.148	0	1.00	0.15	0.85
	420	0.99	0.15	0.85

Note: Data normalized and reported as moles of cation per formula unit (f.u.).

account by adoption of an integral breadth method relating the crystalline size, expressed as the average apparent diameter ε, with the mean lattice strain, η, by the relation

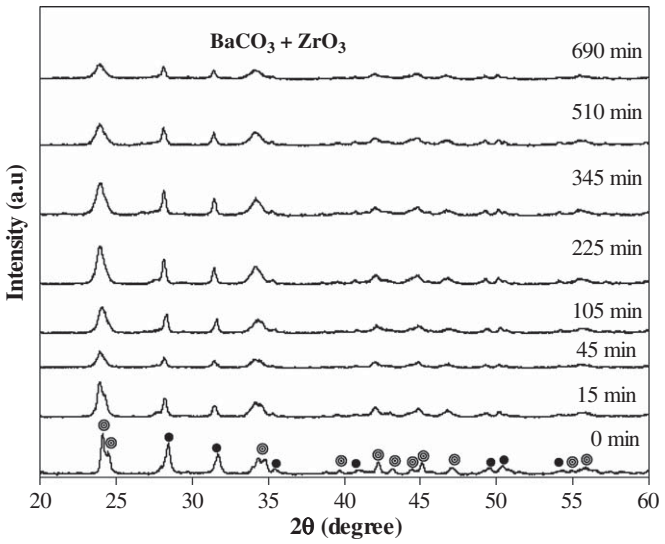

Fig. 3. Evolution of powder X-ray diffraction patterns with milling time for $BaZr_{1-x}Y_xO_{3-\delta}$ composition $x = 0$ for $BaCO_3$+ZrO_2 precursors. The markers identify: (◎) barium carbonate; (●) monoclinic zirconia.

Table 2
Crystallite size, mean lattice strain and mean apparent strain calculated from Williamson–Hall (W–H) plots for $x = 0$, 0.058 and 0.148 compositions, with 420, 300 and 420 min of milling time, respectively, and comparison with crystallite size observed by TEM.

x	Crystallite size (W–H), ε (nm)	Crystallite size (TEM) (nm)	e_{rms} ($\times 10^{-4}$)	Lattice parameter (Å) ± 0.001
0	24 ± 2	14 ± 4	4.6 ± 0.3	4.187
0.058	27 ± 3	22 ± 5	2.4 ± 0.7	4.201
0.148	26 ± 4	18 ± 2	2.1 ± 1.1	4.220

Table also includes lattice parameters of compositions sintered at 1250 °C for 5 h.

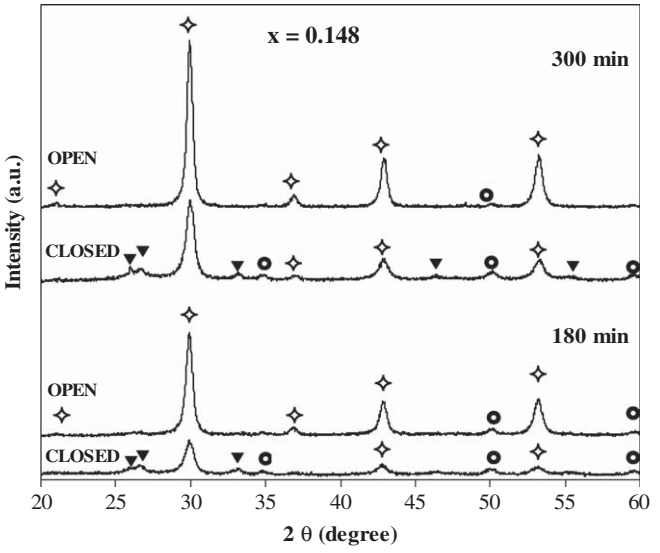

Fig. 4. XRD patterns highlighting the impaired rate of perovskite phase formation when the formed oxygen is prevented from being released by keeping the vial closed. Composition $BaZr_{1-x}Y_xO_{3-\delta}$, $x = 0.148$. (▼) barium peroxide; (O) yttria doped zirconia; (✧) perovskite phase.

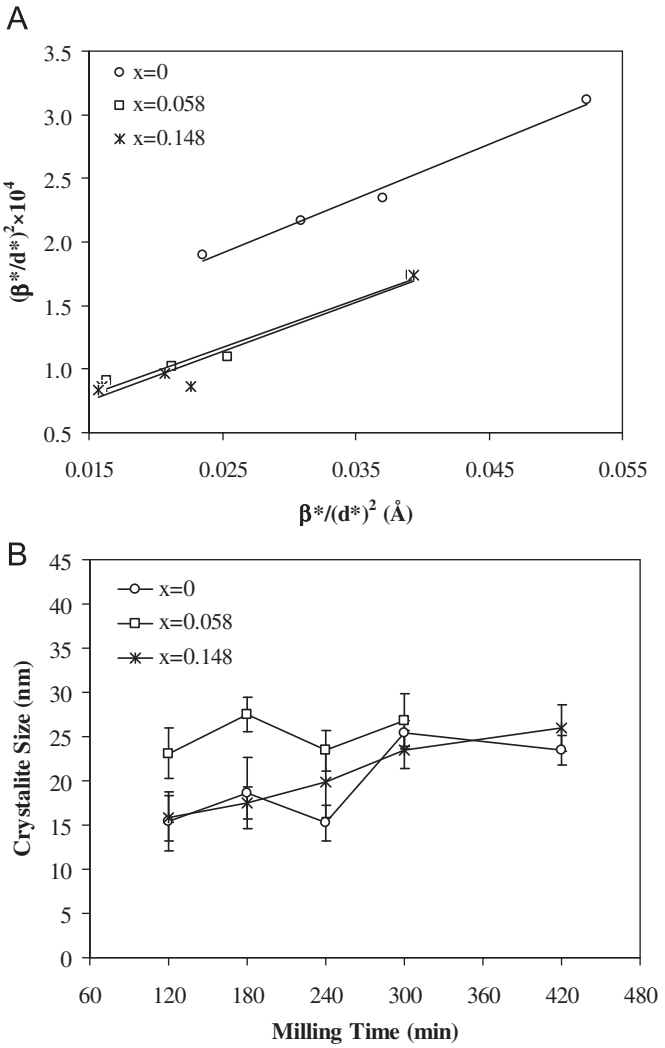

Fig. 5. Williamson–Hall plots (A) shown for compositions, $x = 0$, 0.058 and 0.148 with 420, 300 and 420 min of milling time, respectively. Average crystallite size (B) determined from XRD plotted as a function of milling time.

$$\left(\frac{\beta^*}{d^*}\right)^2 \approx \frac{1}{\varepsilon}\left(\frac{\beta^*}{d^{*2}}\right) + \left(\frac{\eta}{2}\right)^2 \quad (2)$$

where β^* is the integral breath and d^* the interplanar distance, both in reciprocal space units [22]. The representation of β^* and d^* according to Eq. (2), known as the Willamson–Hall plot, is illustrated in Fig. 5A. Linear regression of the Williamson–Hall plot allows the crystallite size (Fig. 5B) and the mean lattice strain (Table 2) to be estimated. The crystallite size shows a slight increase with increasing milling time. The crystallite size of all materials is in the order of 15–35 nm. These values agree well with crystallite sizes determined from TEM images, Table 2. Some example bright field TEM images are shown in Fig. 6. These images also demonstrate that the crystallites are essentially spherical in shape, a geometry which has previously been suggested to favour ceramic processing [3]. Mean apparent strain values, expressed as a root mean square strain, $e_{rms} \approx \eta/5$ [22] (Table 2), are about one order of magnitude lower than those reported for lanthanum oxyapatites [24] or manganese-substituted calcium titanate [23], both compounds with structures of lower symmetry. This observation suggests that the strains induced by milling are more easily relaxed in the cubic barium zirconate structure. It is perhaps interesting to note that strain decreases with increasing Y doping. This could be due to the introduction of oxygen vacancies.

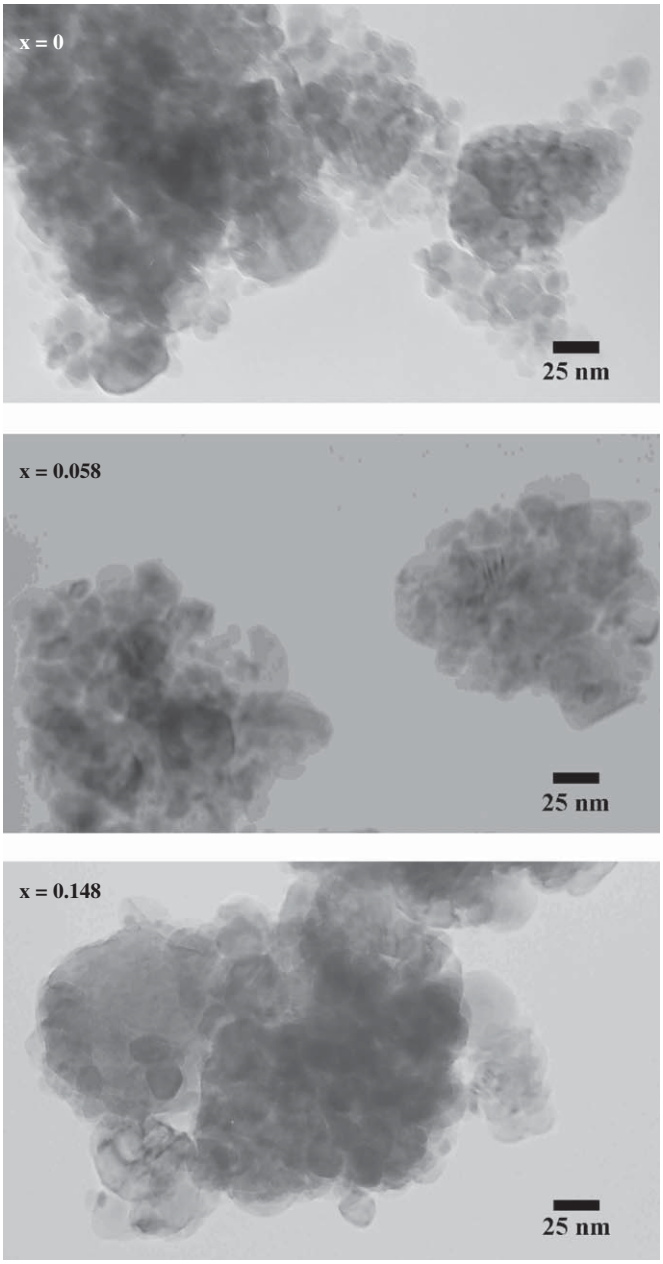

Fig. 6. TEM image collected for samples $x = 0$, 0.058 and 0.148, milled for 420, 300 and 420 min, respectively.

3.3. Carbonate formation

As noted in the introduction, the formation of $BaCO_3$ as an impurity phase on decomposition of organics is a common drawback of soft chemical synthesis routes. The formed $BaCO_3$ requires additional calcinations steps to remove and may add to compositional inhomogeneity. Moreover, the requirement of a separate calcination step may also lead to powder coarsening, defeating the primary purpose of the soft chemical synthesis route. Fig. 1 has shown that the mechanosynthesized powders do not exhibit $BaCO_3$ under the limit of resolution of XRD. The FTIR technique, in contrast, offers much higher sensitivity with which to detect $BaCO_3$ in these materials and is used in Fig. 7 to further

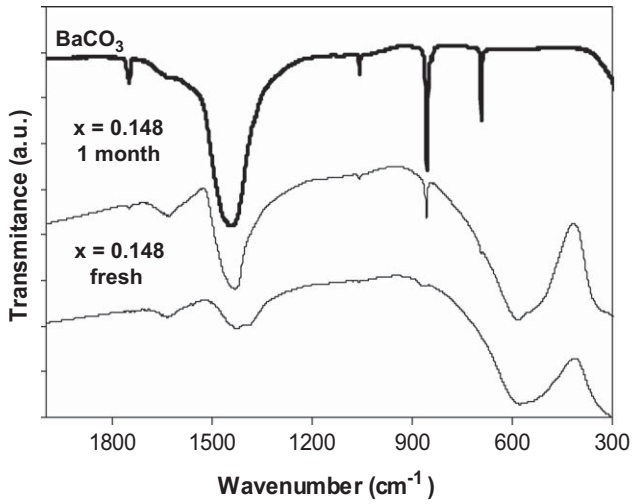

Fig. 7. Comparison between IR transmission spectra of undried $BaCO_3$ commercial powder with mechanosynthesized $BaZr_{0.852}Y_{0.148}O_{3-\delta}$ powder after exposure to atmospheric conditions for 1 month, and fresh mechanosynthesised $BaZr_{0.852}Y_{0.148}O_{3-\delta}$ powder.

demonstrate that mechanosynthesis offers a method of producing $BaZrO_3$-related materials with very low contaminations of $BaCO_3$. Typical absorption bands attributed to the vibrations in the CO_3^{2-} anion are located within the 1800–400 cm^{-1} region. These bands are shown in Fig. 7 for an undried commercial $BaCO_3$ powder for comparative purposes. The strong broad absorption centred at about 1435 cm^{-1} can be connected with the asymmetric stretching vibrations, while sharp absorption bands at approximately 848 and 688 cm^{-1} can be assigned to out of plane bending vibrations and in plane vibrations, respectively [25]. A weak absorption band at 1072 cm^{-1} can also be observed due to symmetric stretching vibrations, while a broad absorption band at 1460 cm^{-1} has been assigned to water uptake and OH bending [26]. Comparison of the FTIR spectrum of $BaCO_3$ with the spectrum of the freshly made composition $BaZr_{0.852}Y_{0.148}O_{3-\delta}$ shows only very small traces of $BaCO_3$ in the mechanosynthesized powder (bands at 848 and 1435 cm^{-1}), which may be a remnant from the commercial barium peroxide precursor used in this study. Again it should be stressed that this level of concentration is below the detection limit of XRD. Fig. 7 additionally shows the absorption spectrum of a mechanosynthesized $BaZr_{0.852}Y_{0.148}O_{3-\delta}$ powder after exposure to atmospheric conditions for 1 month. Clearly, the quantity of $BaCO_3$ impurity has increased substantially, with characteristic absorption bands of CO_3^{2-} now observable at 697, 859 and 1076 cm^{-1}. The broad absorption peak at around 1460 cm^{-1} also exhibits increased intensity. It is interesting to question whether such instability against carbonation is a generic problem related to nanoscale $BaZrO_3$ powders, especially as studies of the longevity of such nanopowders against carbonation are scarce. One article that can be found documents a similar increase of $BaCO_3$ content on standing of nanopowders, which the authors suggest may be related to incomplete reaction [8]. As the current results also show incomplete reaction due to trace amounts of $BaCO_3$ in the commercial BaO_2 precursor, it may be plausible that improvement of the purity of the BaO_2 precursor could improve the long term stability of the current nanopowders.

3.4. Densification

Previously, authors have shown that density in $BaZrO_3$ is inversely related to particle size [3]. The current mechanosynthesis results show the formation of spherical crystallites with sizes in the region of 15–35 nm; properties that should favour densification in the current materials. Fig. 8, therefore, explores densification and grain growth for compositions $x = 0$, 0.058 and 0.148 as a function of sintering temperature. Dwell time at each temperature is 5 h. An increase in grain size can be observed for sintering temperatures in excess of 1500 °C for all compositions (Fig. 8A). Grain growth, however, is much greater in the case of $BaZrO_3$, $x = 0$ (~9 μm at 1600 °C), than for the aliovalent doped compositions, $x = 0.058$ and 0.148 (~1 μm). One should note that this is an interesting phenomenon as it demonstrates that the

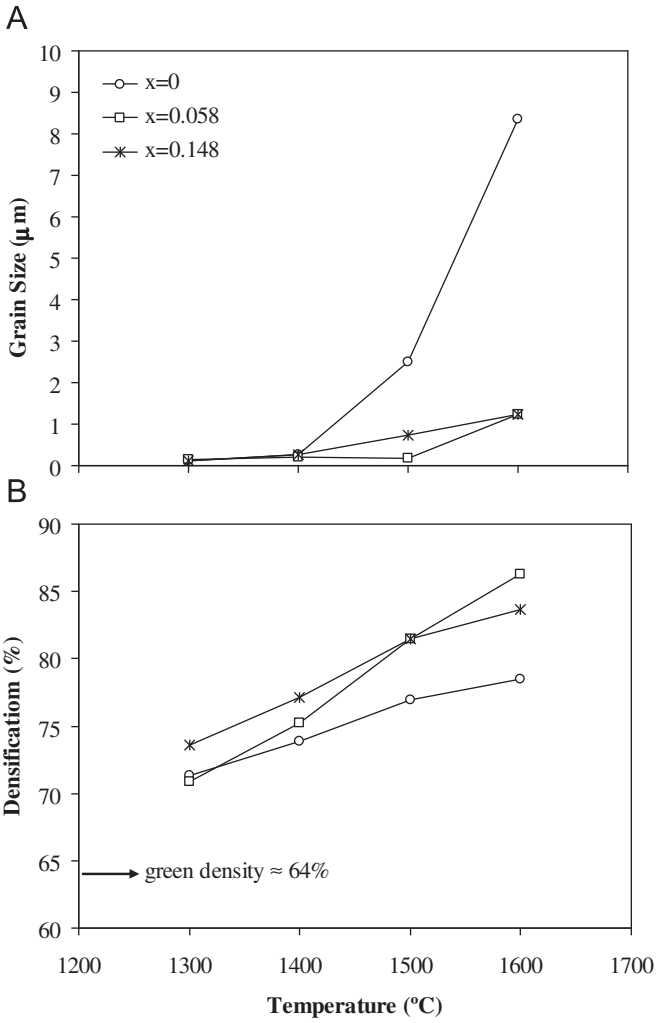

Fig. 8. Grain size (A) and densification (B) for $BaZr_{1-x}Y_xO_{3-\delta}$ ceramics as a function of sintering temperature.

Table 3
Comparison of sample density under different sintering regimes, for samples covered with sacrifical powder of the same composition or uncovered.

x	1500 °C, 5 h uncovered	1500 °C, 5 h covered	1500 °C, 10 h covered	1600 °C, 5 h uncovered	1600 °C, 5 h covered
0	77.0	83.7	90.4	78.5	94.0
0.058	81.5	86.5	88.7	86.3	92.1
0.148	81.5	88.9	90.2	83.7	90.0

Values quoted are %theoretical density for $x = 0$, 0.058 and 0.148 compositions, with 420, 300 and 420 min of milling time, respectively.

Table 4
Comparison of density of mechanosynthesized composition $x = 0.148$ with 420 min of milling time with literature values for $BaZr_{1-x}Y_xO_{3-\delta}$ prepared by a wide range of synthesis techniques for samples sintered under comparable conditions.

x	Preparation method	%ThD	T (°C)	Ramp rate (°C/min)	Dwell (h)	Particle size (nm)	Pressing conditions (MPa)	Covered	Ref.
0.1	Sol–gel–acrylates	95	1500	1.5	15	<20	n/a, vaccum 370	Yes	[13]
0.1	Spray pyrolysis	91	1500	n/a	1	250	Uniaxial, 170	n/a	[17]
0.1	Spray pyrolysis	68	1500	n/a	n/a	n/a	n/a, 200	n/a	[1]
0.1	Sol–gel	65	1500	n/a	n/a	n/a	n/a, 200	n/a	[1]
0.1	Solid state	64	1500	n/a	n/a	n/a	n/a, 200	n/a	[1]
0.1	Spray dried	59	1500	n/a	n/a	n/a	n/a, 200	n/a	[1]
0.148	Mechanosyn.	90	1500	5	10	15–35	Isostatic, 200	Yes	This work
0.2	Sol–gel–alkoxides	99	1500	n/a	20	3–5	Anvil, 4000	n/a	[29]
0.2	Sol–gel polyacrymide	95	1500	n/a	10	n/a	Isostatic, n/a	Surface removed	[12]

Values quoted are %theoretical density (n/a = not available data).

formation of oxygen vacancies does not enhance grain growth in these materials. A similar phenomenon has been noted by Chen et al. [27] for doped cerias where the formation of oxygen vacancies by aliovalent doping also does not enhance grain growth. Chen et al. suggested that the negative impact of solute drag caused this effect. As comparable aliovalent dopant enrichment of crystallite interfaces has also been observed in the current materials for nanoscale powders [28], a similar phenomenon may be acting in the present system. It also should be noted that a high grain growth in composition $x = 0$, does not relate to a higher density, i.e grain growth occurs without shrinkage. In fact, data for yttrium-substituted materials indicate much higher densification rates (Fig. 8B). Additional improvements in density would be expected on control of BaO-loss on sintering, as demonstrated by Schober et al. [12] and also by Haile et al. [4], for example by covering the samples with sacrificial powder of the same nominal composition [4]. The result of this process is documented in Table 3. In every case covering the samples leads to an increase in final density in agreement with these authors. Samples with approximately 90% of their theoretical density can be formed by firing at 1500 °C for 10 h, with further improvements possible by increasing sintering temperature to 1600 °C for 5 h. It should be noted that the composition $x = 0$ exhibits the largest gains in density on prevention of Ba-loss. Table 4 summarizes literature values of %theoretical density obtained for aliovalent doped $BaZrO_3$ prepared by a wide range of synthesis techniques for samples sintered under comparable conditions. The densification of the current mechanosynthesized powders betters many previous works documented in the literature and competes well with peak densities reported for materials formed by state of the art soft chemical routes, such as sol–gel or spray pyrolysis, which offer densities lying in the range 90–95% of the theoretical, under similar sintering conditions.

4. Conclusions

High energy milling of barium peroxide with high purity ZrO_2, $(ZrO_2)_{0.97}(Y_2O_3)_{0.03}$ or $(ZrO_2)_{0.92}(Y_2O_3)_{0.08}$ precursors at 650 rpm in zirconia vials, leads to mechanochemical reaction and the formation of perovskite $Ba(Zr_{1-x}Y_x)O_{3-\delta}$ powders at room temperature for the compositional range $x = 0$, 0.058 and 0.148, respectively. Phase purity is obtained for compositions $x = 0.058$ and 0.148 after milling times of 240 and 420 min, respectively. Composition $x = 0$ shows incomplete mechanochemical reaction even after extended milling times. This was suggested to be due to incomplete reaction resulting from trace impurities of $BaCO_3$ in the commercial BaO_2 precursor. The use of $BaCO_3$ as a starting reagent does not allow the formation of the perovskite phase for any composition. The use of nylon vials rather than hard zirconia vials do not allow the production of the perovskite phase for even the most reactive reagents. Prevention of release of formed oxygen is shown to impede the mechanochemical reaction. The formed perovskite crystallites are spherical in shape with an average size determined from XRD of ca. 30 nm in agreement with transmission electron microscopy observations. A spherical crystallite shape at the nanoscale allows highly competitive densification levels when compared to $BaZrO_3$-based materials formed by alternative synthesis techniques in the literature under similar sintering conditions. Higher densities can be achieved by preventing Ba-loss by covering the samples with sacrificial powder of the same composition. FTIR spectra demonstrate that contamination levels of $BaCO_3$ in the mechanosynthesized powders are very low offering an important advantage over many common alternative low temperature synthesis routes. These advantages together with the use of cheap precursors, fast preparation times, and the absence of pollutant gases demonstrate mechanosynthesis to be a highly attractive method for the formation of $BaZrO_3$-related nanopowders.

Acknowledgments

This work was supported by the FCT, Portugal (projects PTDC/CTM/66243/2006, POCI/CTM/59727/2004) and FAME NoE (Brussels).

References

[1] A.K. Azad, C. Savaniu, S. Tao, S. Duval, P. Holtappels, R.M. Ibberson, J.T.S. Irvine, J. Mater. Chem. 18 (2008) 3414.
[2] S. Imashuku, T. Uda, Y. Awakura, Electrochem. Solid State Lett. 10 (10) (2007) B175.
[3] B. Guillaume, F. Boschini, I. Garcia-Cano, A. Rulmont, R. Cloots, M. Ausloos, J. Eur.. Ceram. Soc. 25 (2005) 3593.
[4] P. Babilo, T. Uda, S.M. Haile, J. Mater. Res. 22 (5) (2007) 1322.
[5] S.M. Haile, G. Staneff, H. Ryu, J. Mater. Sci. 36 (2001) 1149.
[6] B. Robertz, F. Boschini, R. Cloots, A. Rulmont, Int. J. Inorg. Mater. 3 (2001) 1185.
[7] S.B. Reddy, K.P. Rao, M.S.R. Rao, Scr. Materialia 57 (2007) 591.
[8] F. Boschini, A. Rulmont, R. Cloots, B. Vertruyen, J. Eur. Ceram. Soc. 29 (2009) 1457.
[9] Y.V. Kolen'ko, A.A. Burukhin, B.R. Churagulov, N.N. Oleinikov, A.S. Vanetsev, Inorg. Mater. 38 (2002) 252.
[10] P.P. Phulé, D.C. Grundy, Mater. Sci. Eng. B 23 (1994) 29.
[11] R.B. Cervera, Y. Oyama, S. Yamaguchi, Solid State Ionics 178 (2007) 569.
[12] A. Magrez, T. Schober, Solid State Ionics 175 (2004) 585.
[13] Z. Khani, M. Taillades-Jacquin, G. Taillades, M. Marrony, D.J. Jones, J. Rozière, J. Solid State Chem. 182 (2009) 790.
[14] A. Sin, B. El Montaser, P. Odier, J. Am. Ceram. Soc. 85 (8) (2002) 1928.
[15] A.-M. Azad, S. Subramaniam, Mater. Res. Bull. 37 (2002) 85.
[16] M.M. Bućko, J. Obłąkowski, J. Eur. Ceram. Soc. 27 (2007) 3625.
[17] P.A. Stuart, T. Unno, R. Ayres-Rocha, E. Djurado, S.J. Skinner, J. Eur. Ceram. Soc. 29 (2009) 697.
[18] G. Taglieri, M. Tersigni, P.L. Villa, C. Mondelli, Int. J. Inorg. Mater. 1 (1999) 103.
[19] T. Hungría, A. Castro, J. Alloys Compd. 436 (2007) 266.

[20] S. Ohara, A. Kondo, H. Shimoda, K. Sato, H. Abe, M. Naito, Mater. Lett. 62 (2008) 2957.
[21] V.M. Marchev, G.G. Gospodinov, D.G. Stoyanov, Russ. J. Gen. Chem. 69 (3) (1999) 360.
[22] J.I. Langford, Defect and microstructure analysis by diffraction, in: P. Snyder, F. Fiala, H. Bunge (Eds.), IUCr Monographs on Crystallography, vol. 10, Oxford University Press, Oxford, 1999, p. 59.
[23] P. Gonçalves, J. Canales-Vázquez, F.M. Figueiredo, Bol. Soc. Esp. Ceram. 47 (2008) 233.
[24] E. Rodríguez-Reyna, A.F. Fuentes, M. Maczka, J. Hanuza, K. Boulahya, U. Amador, J. Solid State Chem. 179 (2006) 522.
[25] P. Pasierb, S. Komornicki, M. Rokita, M. Rekas, J. Mol. Struct. 596 (2001) 151.
[26] P. Colomban, F. Romain, A. Neiman, I. Animitsa, Solid State Ionics 145 (2001) 339.
[27] P.-L. Chen, I.-W. Chen, J. Am. Ceram. Soc. 77 (9) (1994) 2289.
[28] B. Groß, Ch. Beck, F. Meyer, Th. Krajewski, R. Hempelmann, H. Altgeld, Solid State Ionics 145 (2001) 325.
[29] R.B. Cervera, Y. Oyama, S. Miyoshi, K. Kobayashi, Y. Yagi, S. Yamaguchi, Solid State Ionics 179 (2008) 236.